IEEE TRANSACTIONS ON

ELECTRON DEVICES

A PUBLICATION OF THE IEEE ELECTRON DEVICES SOCIETY

DECEMBER 2014 VOLUME 61 NUMBER 12 IETDAI (ISSN 0018-9383)

(Contents Continued on Page 3917)

(Contents Continued from Front Cover)

Compound Semiconductor Devices

Memory Devices and Technology

Thin Film Transistors

Optoelectronics, Displays, and Imaging

Solid-State Power and High Voltage Devices

Materials, Processing and Packaging

(Contents Continued on Page 3918)

(Contents Continued from Page 3917)

Solid State Device Phenomena

Molecular and Organic Devices

Sensors and Actuators

Vacuum Electron Devices

Emerging Technologies and Devices

BRIEF PAPERS

Modeling of Liquid Nuclei Generation for Field-Emission Silicon Nanocathode

Vladimir G. Danilov, Roman K. Gaydukov, Vadim I. Kretov, and Vadim Yu. Rudnev

***Abstract*— This paper presents the results of mathematical modeling of heat transfer in the field emission process in a conic cathode of small dimensions with its possible melting considered. It is shown that the possibility of melting is determined by the cathode vertex angle. The melting is modeled in the framework of the phase field system using the proposed methods for the formation of the liquid phase zone.**

***Index Terms*— Field emission, heat transfer, melting and solidification, numerical simulation.**

I. Introduction

In THIS paper, we continue to study of the field emission of electrons, which was started in [1] and [2]. Here, in addition to [1] and [2], we stress that the possibility of melting is determined by the cathode vertex angle (if the upper base, height, and applied voltage are fixed). In our model, we actually consider the effects on the interface between the solid and liquid phases if there are such effects, the Nottingham effect, and the Joule heat, but we neglect the radiation because of its relative smallness. The melting is modeled in the framework of the phase field system (the first two equations) and charge conservation law [1], [2]

$$\frac{\partial\theta}{\partial t} - \hat{k}\triangle\theta = -\frac{1}{2}\frac{\partial\varphi}{\partial t} + \frac{t_0 j^2}{l\rho\sigma_e} \tag{1}$$

$$\varepsilon\hat{\alpha}\frac{\partial\varphi}{\partial t} - \varepsilon\hat{\beta}^2\triangle\varphi = \frac{1}{\varepsilon}(\varphi-\varphi^3) + \chi(1-\varphi^2)(\theta-\theta_0) \tag{2}$$

$$\operatorname{div} j = 0. \tag{3}$$

Here, $\triangle$ is the Laplace operator in spherical coordinates (Fig. 2); $\hat{k} = kt_0/r_0^2$; $\hat{\alpha} = cr_0/(\mu l t_0)$; $\hat{\beta} = \sigma\theta_0/(l\rho r_0)$; $k = \lambda/(\rho c)$; $\theta_0 = cT_0/l$; θ is the dimensionless temperature related to the temperature T in Kelvins as $\theta = cT/l$; c is the specific heat capacity; l is the latent heat of melting; r_0 is the characteristic length; λ is the specific thermal conductivity; ε is a small parameter; χ is a parameter equal to $1/\sqrt{2}$ [3]; ρ is the density; t_0 is the characteristic time; k is the thermal diffusivity; $j = -\sigma_e \operatorname{grad}\Psi$ is the current density; σ_e is the specific conductance; Ψ is the electric potential; T_0 is the melting temperature; and μ is the kinetic growth coefficient. The values of these parameters used in our model were taken from [4], [5], and [6], and are presented in Table I.

Manuscript received January 31, 2014; revised August 29, 2014; accepted September 26, 2014. Date of publication October 21, 2014; date of current version December 9, 2014. This work was supported by the Basic Research Program of the National Research University Higher School of Economics, Moscow, Russia. The review of this paper was arranged by Editor R. Carter.

V. G. Danilov and V. I. Kretov are with the National Research University Higher School of Economics, Moscow 101000, Russia (e-mail: vgdanilov@mail.ru; vadim.kretov@gmail.com).

R. K. Gaydukov and V.Yu. Rudnev are with the National Research University Higher School of Economics, Moscow 101000, Russia, and also with the Moscow Technical University of Communications and Informatics, Moscow 111024, Russia (e-mail: roma1990@gmail.com; vrudnev78@mail.ru).

Digital Object Identifier 10.1109/TED.2014.2361168

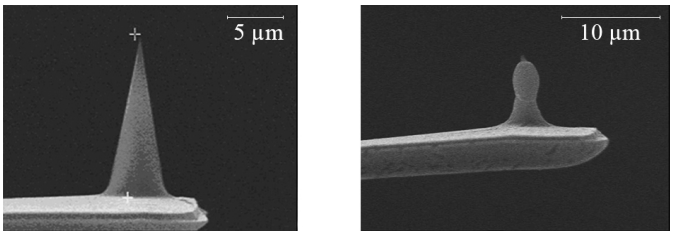

Fig. 1. Scanning Electron Mircroscope (SEM) image of the nanocathode from [7]. (a) Before melting. (b) After partial melting.

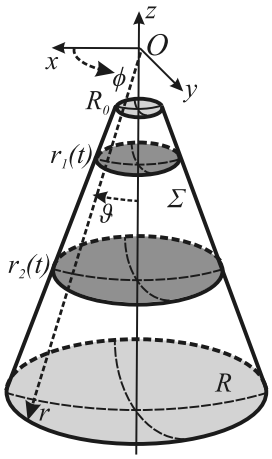

Fig. 2. Nanocathode model.

The cathode is a truncated cone shown in Fig. 2. The cathode geometric dimensions (Table I) correspond to the dimensions of the cathode used in experiments [7].

The system of (1)–(3) is supplemented with the following boundary conditions:

$$\left.\frac{\partial\theta}{\partial r}\right|_{r=R_0} = \frac{c}{l}\frac{r_0}{\lambda}\frac{j_e}{e}E \tag{4}$$

$$\left.\frac{\partial\theta}{\partial r}\right|_{r=R} = \gamma \tag{5}$$

$$\left.\frac{\partial\theta}{\partial \mathbf{n}}\right|_{\Sigma} = 0, \quad \frac{\partial\varphi}{\partial\mathbf{n}} = 0 \tag{6}$$

Here, $\varphi = \varphi(r, \phi, \vartheta, t, \varepsilon)$ is the function of order determining the phase state of the matter: the value -1 corresponds to the solid phase, the value 1 corresponds to the liquid phase, and the intermediate values denote the points at where there is no clearly determinable phase.

TABLE I
PHYSICAL PARAMETERS [4]–[6], GEOMETRIC DIMENSIONS [7], AND THE PARAMETERS USED IN THE DIFFERENCE SCHEME

t_0	100 s	r_0	10^{-5} m
c	678 J/(kg·K)	λ	149 W/(m·K)
σ	0.725 N/m	$k=\lambda/(c\rho)$	9.43×10^{-5} m^2/s
μ	0.5 m/(s·K)	$cr_0/(l\lambda e)$	2.77×10^{-10}
$\hat{\beta}$	0.00133	ε	0.08
θ_0	7.028	$\hat{k}$	94300000
l	1.64×10^5 J/kg	ρ	2330 kg/m^3
T_0	1683 K	$\hat{\alpha}$	1
R_0	0.0022	$t_0/(l\rho)$	2.62×10^{-7}
R	1.0033	γ	$-2\cdot10^{-10}$

where (4) is the boundary condition on the cathode upper base which models the cooling due to the Nottingham effect [8], E is the energy of emitted electrons (7); (5) models the heat removal from the cathode lower base, and (6) is the heat insulation condition and the assumption that phase transaction boundary is orthogonal to Σ (if exists). Here, j_e is the emission current density, defined by [9]–[12]

$$\begin{aligned} j_e = k_1 &\int_{-\infty}^{I_b} \ln\left(1+e^{(W_F-W)/k_BT}\right) \\ &\times\exp\left(-\frac{4\sqrt{2m_e|W|^3}}{3\hbar eE_F}\upsilon(y^{\mathrm{Si}})\right)dW \\ +k_1 &\int_{I_a}^{W_l^{\mathrm{Si}}} \ln\left(1+e^{(W_F-W)/k_BT}\right) \\ &\times\exp\left(-\frac{4\sqrt{2m_e|W|^3}}{3\hbar eE_F}\upsilon(y^{\mathrm{Si}})\right)dW \\ +k_1 &\int_{W_l^{\mathrm{Si}}}^{\infty} \ln\left(1+e^{(W_F-W)/k_BT}\right)dW \end{aligned}$$

where $k_1=(4\pi em_ek_BT)/h^3$, $I_b=-(\psi+\nu E_F^{4/5}+W_g)$; $I_a=-(\psi+\nu E_F^{4/5})$; m_e is the electron mass; k_B is the Planck constant; h is the Planck constant; W_g is the forbidden bandwidth; W_F is the Fermi energy; ψ is the conduction bandwidth; $\varepsilon_{\mathrm{Si}}$ is the dielectric permittivity of silicon; E_F is the external field; $\nu=4.5\cdot10^{-7}\varepsilon_{\mathrm{Si}}^{-2/5}$; and

$$y^{\mathrm{Si}}=\sqrt{\frac{\varepsilon_{\mathrm{Si}}-1}{\varepsilon_{\mathrm{Si}}+1}}\frac{\sqrt{e^3E_F}}{|W|},\quad W_l^{\mathrm{Si}}=-\frac{\varepsilon_{\mathrm{Si}}-1}{\varepsilon_{\mathrm{Si}}+1}\sqrt{e^3E_F}$$
$$\upsilon(y)\approx0.95-1.03y^2$$

where e is the electron charge. The energy of emitted electrons E is calculated by [9]

$$E=\begin{cases}-0.0589529\,\theta\,\mathrm{ctg}(14.6137\,\theta), & \theta\leqslant\theta^*\\ 4.42871+0.0417038\,\theta & \\ \quad+\dfrac{-21.8518+0.25058\,\theta}{4.92306+(-1+9.30338\,\theta)^{3.48481}}, & \theta>\theta^*.\end{cases}\tag{7}$$

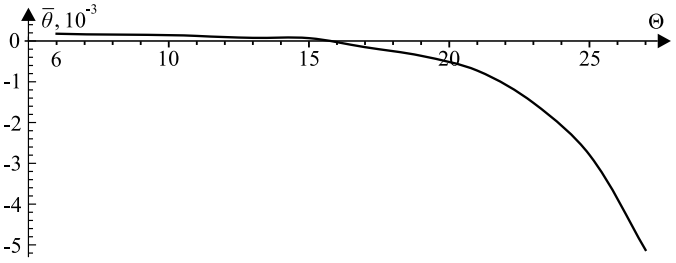

Fig. 3. Dependence of the temperature on the cathode vertex angle Θ.

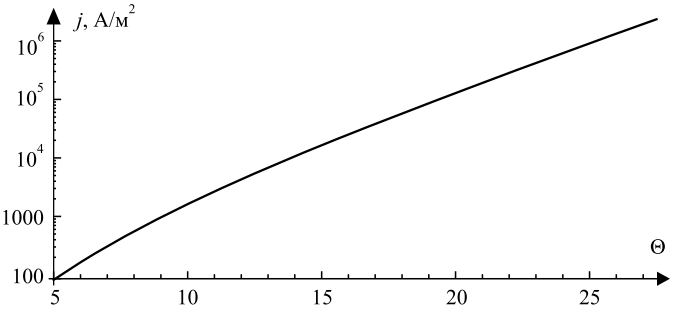

Fig. 4. Emission current density. The ordinate axis is logarithmic.

Here, $\theta^*=51c/l$, and $\mathbf{n}$ is the normal to the surface directed from the solid phase to the liquid phase. We also note that the term responsible for the radiation can be added to condition (4) determining the derivative $(\partial\theta/\partial r)\big|_{r=R_0}$, but we neglect this term because of its smallness. The external field is determined by the voltage $U=4$ V applied to the cathode.

The facts that the equations contain a large dimensionless coefficient $\hat{k}$ and a small coefficient $\hat{\alpha}$ (Table I) lead to known difficulties, and these problems were discussed in [1] and [2]. The fact that $\hat{k}$ is large and the boundary conditions imply that the temperature and the function of order slightly depend on the azimuthal angle (and this is confirmed by numerical experiments). The problem under study is symmetric with respect to the polar angle as well. The smallness of the coefficient $\hat{\alpha}$ means that the Allen-Cahn equation (2) is almost stationary, and therefore, to solve it numerically using a difference scheme, we assume that $\hat{\alpha}=1$ and perform iterations, thus modeling the stationary state approach.

In this paper, we present the photos [7] (Fig. 1) which show that the cathode melting zone (the area where the cathode loses its shape) is close to the cathode vertex but does not approach it.

All statements of this paper are illustrated by graphs. The dimensionless temperature $\bar{\theta}$ shown in the plots is $\bar{\theta}=(T-T_0)c/l$, where T is the temperature in K and T_0 is the melting temperature in K. The graphs illustrate the temperature on the cathode axis, and Θ on the graphs in Figs. 3 and 4 is half the cathode vertex angle. Since the temperature in the cathode equalizes rapidly, its variations are small.

II. DEPENDENCE OF THE TEMPERATURE ON THE VERTEX ANGLE

This section completes the results obtained in [1] and [2]. Here, we present the temperature dependence on the cathode vertex angle.

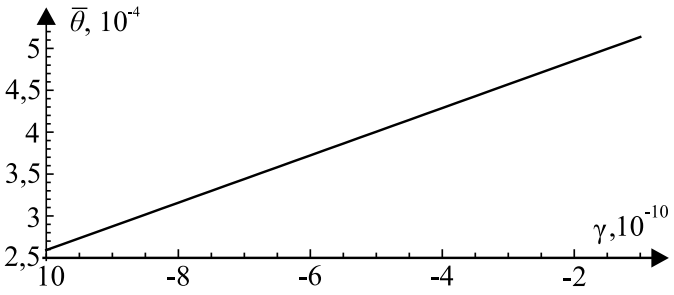

Fig. 5. Dependence of the cathode lower base temperature on the coefficient in the boundary condition (5).

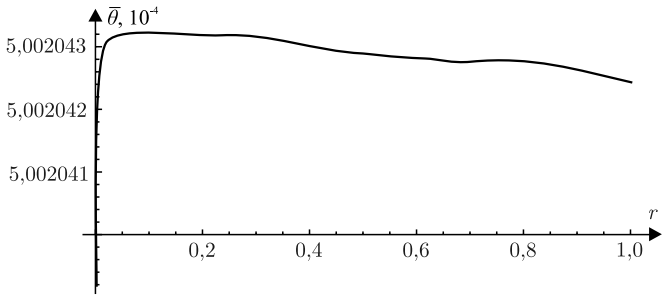

Fig. 6. Temperature after the melting temperature is exceeded without incorporating a nucleus. The extreme left point corresponds to the cathode upper base with the coordinate $r = 0.0022$.

The dependence of the temperature and the emission current on the cathode vertex angle is shown in Fig. 3. The melting occurs at the angle value ($\Theta = 10°$) given in [7].

The computations were performed for the angles Θ varying from 6 to 27.5°, while the cathode height and the upper base area remained constant. In this section, the temperature θ was calculated starting from a constant $\hat{\theta} < \theta_0$ after a hundred of time steps. Time step is equal to 10^{-5}. The temperature was taken at the center of the upper base. The results are presented in Fig. 3.

The dependence of the current density obtained in the model on the cathode vertex angle is shown in Fig. 4.

Prior to passing to the next section, we mention some specific features of the temperature characteristic distribution over the cathode (Fig. 6). A strong decay due to the Nottingham effect is clearly seen on the left boundary of graph that corresponds to the cathode upper base. The influence of the heat removal on the cathode lower base is also noticeable, it is illustrated by the right boundary of the graph. Fig. 5 presents the temperature significant dependence on the small value of γ—the heat removal condition in the lower base. The maximum of the temperature in the cathode lies closer to the upper base, because the current density increases as the distance to the vertex decreases, and thus the heating due to the Joule heat also increases. Finally, the total temperature drop is rather small, which can be explained by the large value of the dimensionless coefficient of thermal diffusivity $\hat{k}$ that leads to the temperature fast equalizing in the entire cathode (Fig. 6).

III. Formation of Melting and Crystallization Nuclei in the Model

We assume that at $t = t_0$, the region is occupied by one (solid) phase, i.e., $\varphi = -1$. In this case for $\theta \neq \theta_0$ (where θ_0 is the dimensionless melting temperature), (2) has a nonzero right-hand side, which changes the function of order by a quantity approximately equal to

$$\frac{1}{\hat{\alpha}\varepsilon} \int_{t_0}^{t_0+t} (\theta - \theta_0)\, d\tilde{t} \tag{8}$$

for small variations in t. We note that the values $\varphi = \pm 1$ are stable, $\varphi(1-\varphi^2) > 0$ for $0 < \varphi < 1$, and $\varphi(1-\varphi^2) < 0$ for $-1 < \varphi < 0$.

The contribution of nonlinearity into the variation of φ for small t approximately has the form

$$\frac{1}{\hat{\alpha}\varepsilon^2} \int_{t_0}^{t_0+t} \varphi(1-\varphi^2)\, d\tilde{t}. \tag{9}$$

It is clear that the contribution of (9) due to the multiplier ε^{-2} is greater than the contribution of (8). Therefore, the nonlinearity also suppresses the influence of the temperature small deviations for not very large values of $\theta - \theta_0$, and even in the case where the melting temperature is exceeded, the function φ is still equal to -1. It is clear that such a behavior of the solution contradicts the meaning of the modeled process.

On the other hand, it is known that the new phase formation starts with the appearance of nuclei, i.e., some inhomogeneities resulting in the origination of this new phase [13].

To remove the contradiction with the physical meaning, which is a consequence of the chosen model, we propose our own method for incorporating the nuclei, which is an external method with respect to the phase field system. This method differs from the method proposed in [13], where it is assumed that the nucleus is a small volume of a new phase in the old phase volume. We incorporate a nucleus as an unstable state in a small volume of the old phase, or we can say that we artificially create an unstable mushy region [14] in a small volume of the old phase. Of course, this raises the problem under what conditions a mushy region can be created.

For the Allen–Cahn equation with a right-hand side, which describes the function of order, it is known that, in the case of a homogeneous equation, the states $\varphi = \pm 1$ are stable (this was already discussed above), and the state $\varphi = 0$ is unstable. Therefore, it is natural to assume that the phase nucleus is the region where $\varphi \approx 0$. Then, as follows from physical experiments, some nuclei cause the appearance of a new phase and some nuclei disappear. In the case under study, the phase nuclei have precisely such properties and the nucleus development depends on its size.

Let us determine the conditions of the nucleus development. In our case, the term development means that, on the interval under study, φ takes a value different from the value at the moment of the nucleus appearance. For example, if the value $\varphi \approx 0$ arises from the value $\varphi = -1$, then the nucleus development means the evolution of φ to $+1$, and its death means the evolution to -1. Therefore, the nucleus

development conditions can be formulated in terms of the derivative with respect to time of the integral

$$\iiint_V \varphi(r,t)\,dV \tag{10}$$

where V is the volume of the cathode (of the truncated cone). We first note that

$$\iiint_V f(r,t)\,dV = \int_{R_0}^{R} r^2 f(r,t)\,dr \int_0^{\pi} d\phi \int_{-\Theta}^{\Theta} |\sin\vartheta|\,d\vartheta$$
$$= 2\pi(1-\cos\Theta)\int_{R_0}^{R} r^2 f(r,t)\,dr. \tag{11}$$

The left and right boundaries of the interval of integration are denoted by R_0 and R.

Therefore, when integrating over the layers between the cone (cathode) cross sections by spheres centered at the cone vertex, we always obtain integrals over the radial variable multiplied by the same constant equal to $2\pi(1-\cos\Theta)$. It is clear that this constant can be omitted in all terms.

The derivative of (10) with respect to t can be determined from the balance relation. For this, we integrate the left- and right-hand sides of the equation over the cathode volume, consider (11), and obtain

$$\int_{R_0}^{R} \varepsilon\hat{\alpha} r^2 \frac{\partial\varphi}{\partial t}\,dr - \int_{R_0}^{R} \varepsilon\hat{\beta}^2 \frac{\partial}{\partial r} r^2 \frac{\partial\varphi}{\partial r}\,dr$$
$$= \int_{R_0}^{R} \frac{1}{\varepsilon} r^2(\varphi-\varphi^3)\,dr + \int_{R_0}^{R} \chi r^2(\theta-\theta_0)\,dr. \tag{12}$$

Let us define the class of functions where the nucleus can be chosen. As was shown in [15], the interaction of nonlinear parabolic waves can approximately be described by the sum of simple waves ranging in the strip from -1 to 0. For the Allen–Cahn equation, the simple waves have the form

$$\hat{\varphi}_{\pm}(t,r) = -\left(1+\exp\left(\frac{3t/\sqrt{2}\pm r}{\beta\varepsilon\sqrt{2}}\right)\right)^{-1}.$$

As the nuclei, we consider the family of functions that are sums of simple waves for $t=0$

$$\varphi = A+(A+1)\left[\hat{\varphi}_-(0,r-(r_0+\delta/2))+\hat{\varphi}_+(0,r-(r_0-\delta/2))\right] \tag{13}$$

where r_0 is the nucleus center position, δ is its width, and the constant A determines the maximal value of the nucleus, i.e., for $A>0$, the nucleus takes positive values at the point of maximum, and for $A<0$, the nucleus lies completely inside the strip $[-1,0)$ (Fig. 7).

For $A=2$ and a sufficiently large value of δ, such a function is the simple representative of the gas of kinks introduced in [16]. For $A=1$, the function (13) ranges in the strip $[-1,0)$, and for a small excess of the amplitude A over 1, this function has the form shown in Fig. 7. It is natural to assume that such a function is the liquid phase nucleus in the solid phase.

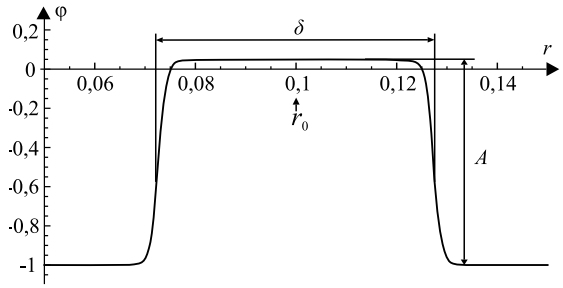

Fig. 7. Melting nucleus, $\varphi=-1$ is a solid phase and $\varphi=1$ is a liquid phase, $-1<\varphi<1$ is an unstable region.

More precisely, the nucleus must satisfy the following conditions.

1) At a temperature greater than the melting temperature, the nucleus must generally grow, i.e., as the time increases, its maximum must attain a value close to $+1$ on an interval (from the standpoint of the properties of the function of order, this means the appearance of a melted layer).
2) When a nucleus is incorporated, the rate of the temperature variation with time must remain unchanged.

Let us present our algorithm of the nucleus incorporation. We calculate the temperature until the time moment t_0 at which it begins to the exceed the melting temperature. At this moment, the computation stops (the process modeling is stopped), and then it starts again with the calculated temperature taken as the initial condition for θ and with φ given by (13).

Using the phase field system equations, we can write the balance equation, i.e., the expression for

$$\frac{d}{dt}\int_{R_0}^{R} r^2\theta\,dr\bigg|_{t=t_0.}$$

We integrate the heat conduction equation (1), consider remark (11), and obtain

$$\frac{d}{dt}\int_{R_0}^{R} r^2(\theta-\theta_0)\,dr = \hat{k}R^2\frac{\partial\theta}{\partial r}\bigg|_{r=R} - \hat{k}R_0^2\frac{\partial\theta}{\partial r}\bigg|_{r=R_0}$$
$$-\frac{1}{2}\int_{R_0}^{R} r^2\frac{\partial\varphi}{\partial t}\,dr + \int_{R_0}^{R} r^2\frac{t_0 j^2}{l\rho\sigma_e}\,dr. \tag{14}$$

We substitute the expression for $\partial\varphi/\partial t$ from (12) into (14), consider that $\partial\varphi/\partial r=0$ for $r=R_0, R$, and obtain

$$\frac{d}{dt}\int_{R_0}^{R} r^2(\theta-\theta_0)\,dr = \hat{k}R^2\frac{\partial\theta}{\partial r}\bigg|_{r=R} - \hat{k}R_0^2\frac{\partial\theta}{\partial r}\bigg|_{r=R_0}$$
$$-\frac{1}{2\varepsilon^2}\int_{R_0}^{R} r^2(\varphi-\varphi^3)\,dr - \frac{1}{2\varepsilon}\int_{R_0}^{R}\chi r^2(\theta-\theta_0)\,dr + \int_{R_0}^{R} r^2\frac{t_0 j^2}{l\rho\sigma_e}\,dr. \tag{15}$$

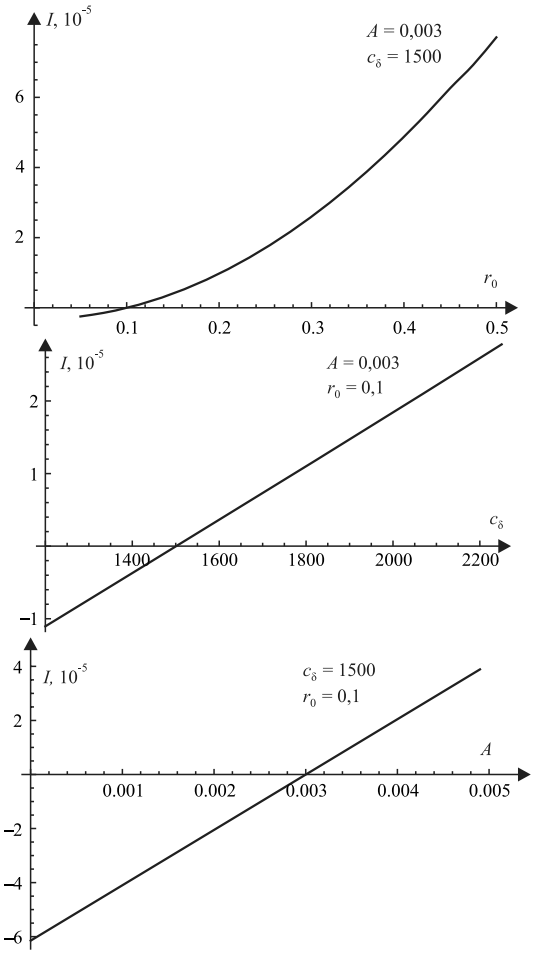

Fig. 8. Dependence of I given by (16) on the nucleus position r_0, width $\delta = c_\delta \varepsilon\beta$, and amplitude A.

Here, we considered that the equation for the function of order φ is solved by the iteration method (Section I). This means that the equation for φ is solved until the derivative $\partial\varphi/\partial t$ becomes sufficiently small. It follows from (15) that all terms except the third are continuous at $t = t_0$ and the third term is discontinuous at $t = t_0$ and its jump is equal to the integral:

$$I = \frac{1}{\varepsilon}\int_{R_0}^{R} r^2(\varphi - \varphi^3)\, dr \tag{16}$$

where φ is a function of the form (13). For the continuity, we must equate this terms with 0. Fig. 8 shows the behavior of I depending on the parameters determining it.

For $t > t_0$, the sum of the third and fourth terms in the right-hand side of (15) is small, because their sum is equal to

$$\frac{d}{dt}\int_{R_0}^{R} r^2\varphi\, dr\bigg|_{t=t_0}$$

and φ is a solution of quasi-stationary equation.

Thus, the main contribution to the right-hand side of (15) is given by the total power of the heat sources, and the nucleus develops if the temperature is positive.

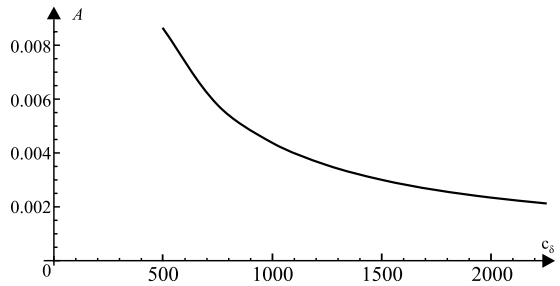

Fig. 9. Dependence of the amplitude A on the nucleus width $\delta = c_\delta \varepsilon\beta$ for $r_0 = 0, 1$ under the condition $I = 0$.

We determine the nucleus parameters r_0, δ, and A starting from the condition that the integral (16) is equal to zero. The parameter A can be determined for given r_0 and δ. Further, it is reasonable to place the nucleus at the point of maximum of the temperature, i.e., r_0 is determined by the condition

$$\theta(r_0) = \max\theta(r)$$

at the time step after which the nucleus is added. Finally, it is necessary to determine δ. We consider the graph of $A(\delta)$ for a fixed r_0 (Fig. 9). We observe that this dependence is nearly hyperbolic, and for the nucleus width, it is reasonable to take the width δ such that the amplitude A varies weakly if this width is exceeded. Then the graph in Fig. 9 is almost independent of the choice of r_0, and for the width we can take, for example, the value $\delta = 1500\varepsilon\beta$.

We model the melting process with incorporation of the liquid phase nucleus under the following assumptions.

The cathode vertex angle is decreased to decrease the influence of the Nottingham effect. In this section, this angle is equal to 11.4°. The same effect can be obtained for the unchanged geometry by decreasing the shape factor in the Nottingham condition.

Moreover, the specific conductivity increases with the temperature in semiconductors in contrast to metals. We assume that this is possible in the transition to the liquid state, when some additional electrons appear in the semiconductors due to the breakage of the interatomic covalent bonds. Therefore, the conductivity increases jumpwise in local melting, which can lead to a decrease in the Joule heat. However, we could not determined the exact value of the conductivity variation. On the other hand, it naturally follows from general considerations that a part of free electrons from the melting zone can increase the emission current density, which implies an increase in the Nottingham effect, i.e., in the energy carried away by the emitting electrons. In our model, we use the formula that describes the Nottingham effect for the electron emission from metals but does not take account of the increase in the flow of emitting electrons. Therefore, we introduce an artificial shape factor, i.e., a correcting coefficient, into this formula, which allows us to regard both of the (hypothetic) phenomena described above, because both of them contribute to the cathode matter cooling. This shape factor is a function of time and is determined by a curve of the form shown in Fig. 10, which allows us to take account of the possible jumpwise increase in the number of electrons. A jump in the Nottingham condition means that the cathode begins to cool

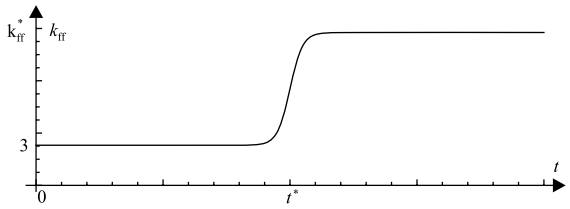

Fig. 10. Dependence $k_{\mathrm{ff}}(t)$, where $t^* = t_3$ is the time of formation of the liquid phase region.

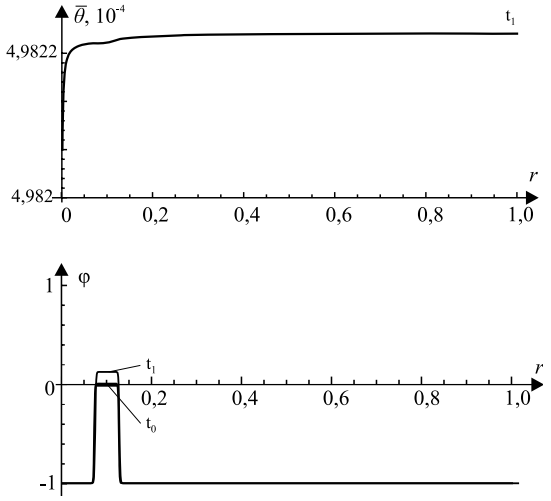

Fig. 11. t_0 is the time moment at which the nucleus is introduced, $\bar{\theta}$ is shown in Fig. 6, and $t_1 > t_0$ is the nucleus development (Fig. 7).

down after melting, which further leads to its solidification and disappearance of the region filled with the liquid phase.

Let us illustrate the above considerations. Fig. 6 presents a typical graph of the temperature exceeding the melting temperature. After several computation steps, we incorporate the nucleus at a certain temperature so that, with the error considered, the calculated temperature exceeds the melting temperature. At this temperature, we incorporate the nucleus (Fig. 11). The temperature in our algorithm is calculated from a given function of order, and therefore, at the first moment after the nucleus incorporation, the temperature remain almost unchanged due to the second condition of nucleation, but its local structure is changed and a parabolic fragment appears (Fig. 11). Moreover, the parabolic fragment of the temperature graph in the region between the phase boundaries is typical of problems with interacting fronts [14]. In Fig. 12, this parabolic fragment is smeared by the action of the Nottingham boundary condition.

It follows from the balance relations that the nucleus develops, as shown in Fig. 12. Finally, the nucleus becomes the liquid phase region at time t_3. After the moment of the nucleus formation, the process of the nucleus development is accompanied with the heat removal [described by the term $-(\partial\varphi/\partial t)/2$ in the right-hand side of the heat conduction equation (1)], and this heat is spent to the phase transition in the cathode matter, and therefore, the temperature during the nucleus development decreases and can be even lower than the melting temperature, just as in Figs. 11, 12.

The further modeling was performed in two versions. In the first version, we start from the above considerations that

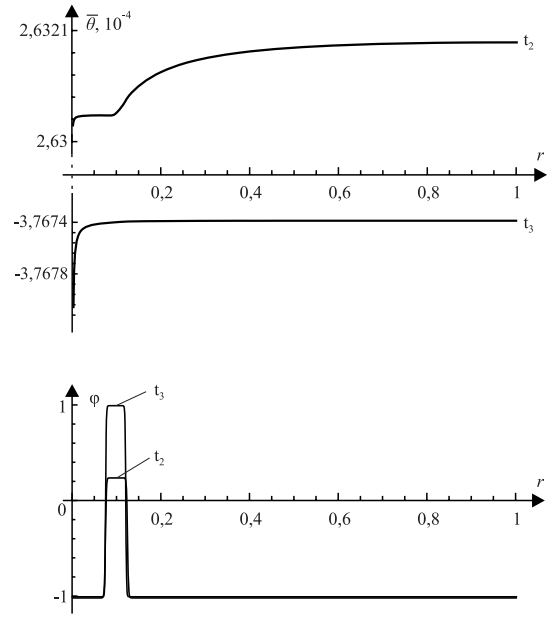

Fig. 12. Nucleus development: $t_2 > t_1$: the nucleus continues to grow; time moment $t_3 > t_2$: the liquid phase region is formed completely (Fig. 7).

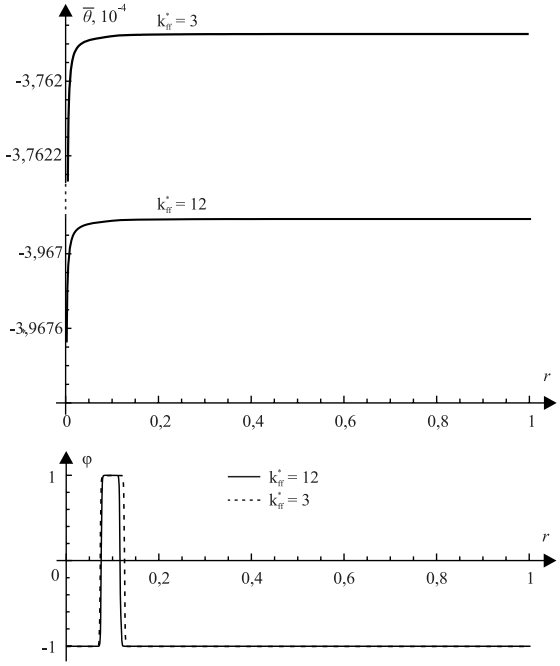

Fig. 13. Time moment $t_4 > t_3$: as the shape factor increases to the value $k_{\mathrm{ff}}^* = 12$, the temperature decreases and the liquid phase region stops to develop; if the shape factor remains unchanged ($k_{\mathrm{ff}}^* = 3$), then the temperature begins to increase and the liquid phase region continues to develop.

the Nottingham effect must increase after the liquid phase formation, which can result in further cooling and collapse of the liquid phase region. For example, we took the shape factor equal to $k_{\mathrm{ff}}^* = 12$. The graphs illustrating the further behavior of the process are shown in Fig. 13. One can see that the temperature actually continues to decrease and the width of the liquid phase region also slightly decreases.

The relative temperature at which the free boundary stops and the nucleus is fractured is related to the position of the free boundary (17). Here, $r_1(t)$ and $r_2(t)$ are the time-dependent

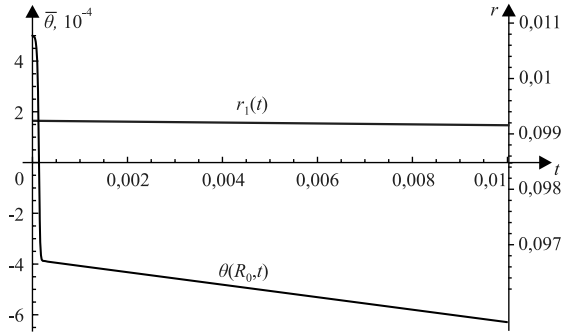

Fig. 14. Time-dependence of the cathode upper base temperature and the position of the free boundary which is the closest to the upper base.

coordinates r of the left and right free boundaries. We see that if the maximum of the temperature lies at a greater distance from the vertex, which is possible in the case of strong cooling on the cathode lower base and weak influence of the Nottingham effect, then the free boundaries stop and the nucleus disappears at a temperature that is closer to the melting temperature than that in the case where the maximum of the temperature is closer to the vertex, as shown in Figs. 7–14 (i.e., for a greater curvature of the phase interface)

$$\left(\theta-\theta_0\right)\Big|_{r=r_1(t)}=-\hat{\beta}\frac{2}{r_1(t)},\quad \left(\theta-\theta_0\right)\Big|_{r=r_2(t)}=\hat{\beta}\frac{2}{r_2(t)}. \quad (17)$$

Fig. 14 shows that the free boundary moves very slowly (it practically does not move) compared with the decrease in the temperature, and therefore, according to condition (17), as the temperature becomes lower than the temperature obtained from this condition (i.e., lower than the value $\theta-\theta_0\approx -0,038$), the liquid phase region begins to narrow and finally disappears. This process is similar to that described (for nonphysical parameters) in [1]. The slow motion of the free boundary can be explained by the presence of the small coefficient $\beta^2\sim 10^{-6}$ in the term with the Laplace operator in the Allen–Cahn equation. Fig. 14 also shows that the temperature first rapidly decreases because of the nucleus growth, and then the decrease becomes slower but still continues due to the increasing shape factor. Moreover, it follows from the conditions under which we add the nucleus that the temperature remains almost the same at the initial time moment after the nucleus addition.

In the second version of the modeling, we do not change the shape factor, and therefore, after the liquid phase region is formed, an insignificant quantity of heat is required for the phase transition because of the slow motion of the free boundaries, and the temperature begins to grow (Fig. 13). Although the temperature in the graph is less than the melting temperature, it still increases and becomes positive in the further modeling. In this case, the liquid phase region continues to expand and will melt the entire cathode in the course of time.

IV. Conclusion

In this paper, it was shown that the thermal characteristics of the process are significantly affected by the cathode vertex angle. The balance relations following from the phase field system are analyzed. This balance is used to propose a heuristic algorithm for incorporating the liquid phase nucleus in the cathode model earlier described in [1] and [2]. In contrast to the preceding works, we here perform calculations with parameters corresponding to the physical parameters of the cathode. Despite the fact that the available experimental data are incomplete, it should be noted that our mode contains only one adjusting parameter, the shape factor, i.e., the coefficient in the formula of the emission current density and one controlling parameter γ modeling the cooling on the cathode lower base.

References

[1] V. G. Danilov, V. Y. Rudnev, and V. I. Kretov, "Simulation of the heat transfer in the nanocathode," *Open J. Appl. Sci.*, vol. 2, pp. 78–81, Dec. 2012.
[2] V. G. Danilov, V. Y. Rudnev, and V. I. Kretov, "Simulation of the heat transmission in the nano–sized cathode," in *Proc. 4th Int. Conf. Differ. Equ. Appl.*, Donetsk, Ukraine, 2012, p. 94.
[3] G. Caginalp, "An analysis of a phase field model of a free boundary," *Archive Rational Mech. Anal.*, vol. 92, no. 3, pp. 205–245, 1986.
[4] W. M. Haynes, *CRC Handbook of Chemistry and Physics*, 94th ed. Boca Raton, FL, USA: CRC Press, 2013.
[5] E. A. Brandes and G. B. Brook, *Smithell's Metals Reference Book*. London, U.K.: Butterworth, 1997.
[6] R. Hull, *Properties of Crystalline Silicon*. London, U.K.: IET, 1999.
[7] N. Dyuzhev, S. Gudkova, M. Makhiboroda, and V. Fedirko, "Study of emission properties of silicon cathodes of different geometry," in *Proc. 12th Sci.-Tech. Conf. Participation Foreign Specialists Vac. Sci. Technol.*, Moscow, Russia, 2005, pp. 221–224.
[8] P. H. Levine, "Thermoelectric phenomena associated with electron-field emission," *J. Appl. Phys.*, vol. 33, no. 2, pp. 582–587, 1962.
[9] J. Paulini, T. Klein, and G. Simon, "Thermo-field emission and the Nottingham effect," *J. Phys. D, Appl. Phys.*, vol. 26, no. 8, pp. 1310–1315, 1993.
[10] R. Stratton, "Theory of field emission from semiconductors," *Phys. Rev.*, vol. 125, no. 1, pp. 67–82, Jan. 1962.
[11] E. L. Murphy and R. H. Good, "Thermionic emission, field emission, and the transition region," *Phys. Rev.*, vol. 102, no. 6, pp. 1464–1473, Jun. 1956.
[12] M. Ding, "Field emission from silicon," Ph.D. dissertation, Dept. Phys., Massachusetts Inst. Technol., Cambridge, MA, USA, 2001.
[13] A. N. Kolmogorov, "On the statistical theory of metal crystallization," *Izvestiya Akademii Nauk SSSR. Ser. Matematicheskaya*, vol. 1, no. 3, pp. 355–359, 1937.
[14] V. G. Danilov, G. A. Omel'yanov, and E. V. Radkevich, "Hugoniot–type conditions and weak solutions to the phase–field system," *Eur. J. Appl. Math.*, vol. 10, no. 1, pp. 55–77, 1999.
[15] V. G. Danilov, V. P. Maslov, and K. A. Volosov, *Mathematical Modelling of Heat and Mass Transfer Processes*. Norwell, MA, USA: Kluwer, 1995.
[16] M. J. Ward and L. G. Reyna, "Resolving weak internal layer interactions for the Ginzburg–Landau equation," *Eur. J. Appl. Math.*, vol. 5, no. 4, pp. 495–523, 1994.

Vladimir G. Danilov received the Ph.D. degree from the Moscow Institute of Electronics and Mathematics, Moscow, Russia, in 1976, and the D.Sc. degree from Moscow State University, Moscow, in 1990.

He is currently a Professor with the National Research University Higher School of Economics, Moscow. His current research interests include nonlinear problems of PDE, asymptotics methods, and mathematical simulation.

Roman K. Gaydukov received the M.S. degree from the Moscow Institute of Electronics and Mathematics, Moscow, Russia, in 2012. He is currently pursuing the Ph.D. degree with the Moscow Technical University of Communications and Informatics, Moscow.

He is currently a Researcher with the National Research University Higher School of Economics, Moscow.

Vadim I. Kretov received the M.S. degree from the Moscow Institute of Electronics and Mathematics, Moscow, Russia, in 2008.

He is currently a Researcher with the National Research University Higher School of Economics, Moscow. His current research interests include mathematical simulation, field emission, and numerical solution of PDE.

Vadim Yu. Rudnev received the Ph.D. degree in mathematical physics from the Moscow Institute of Electronics and Mathematics, Moscow, Russia, in 2005.

He is currently an Associate Professor with the Moscow Technical University of Communications and Informatics, Moscow. His current research interests include modeling, simulation of phase transition in the phase-field model, and simulation of heat transfer in cathodes.